JOURNAL OF CATALYSIS 118, 266–274 (1989)

Elementary Steps in the Formation of Highly Dispersed Palladium in NaY

II. Particle Formation and Growth

S. T. HOMEYER AND W. M. H. SACHTLER[1]

Ipatieff Laboratory, Department of Chemistry, Northwestern University, Evanston, Illinois 60208

Received December 30, 1988; revised March 3, 1989

Calcination conditions which leave Pd ions in Pd/NaY in two reproducible states have previously been defined: Low-temperature calcination (T_C = 250°C) leaves $Pd(NH_3)_x^{2+}$ in supercages, but high-temperature calcination (T_C = 500°C) places Pd^{2+} quantitatively in sodalite cages. It has now been found that the processes which lead to Pd particle formation during reduction with H_2 are entirely different for these two cases. Reduction of Pd ions in supercages results in the formation of primary particles ($d < 7$ Å) which rapidly migrate and coalesce to larger particles, whose migration is impeded by the size of the supercage windows. Reduction of Pd ions in sodalite cages, however, leads to the formation of isolated atoms or dimers which are trapped in these cages. Their subsequent release into the supercage network is an activated process. The ratio of adsorbed hydrogen to reduced palladium, in this case, initially increases with temperature, then passes through a maximum, indicating that isolated Pd atoms are incapable of dissociatively chemisorbing H_2.

INTRODUCTION

A primary goal of recent research on metal/zeolite systems has been to determine the conditions necessary for the formation of highly dispersed metal particles occluded in specific locations within the zeolite matrix. An understanding of the elementary steps involved in particle formation is prerequisite for the determination of the most effective preparation conditions. We have, therefore, characterized metal/NaY catalysts with a combination of chemical (temperature-programmed reduction (TPR), hydrogen desorption (TPD), oxidation (TPO), and H_2 chemisorption) and physical methods (XRD, XPS, EXAFS and IR spectroscopy) (*1–10*).

The available data on Pt and Pd/NaY systems justify the following generalizations: Metal ions migrate during calcination to locations which provide greater electrostatic stabilization and higher coordination to lattice oxygen ions. The extent of migration and the location of metal ions after calcination is determined by size to charge ratios and degree of complexation of the metal ion, the latter being controlled by calcination temperature. Our data show that, for $Pt(NH_3)_4^{2+}$/NaY, a calcination temperature which completely removes ammine ligands and leaves Pt^{2+} ions in the supercages can be found (*1*). However, in the case of $Pd(NH_3)_4^{2+}$/NaY, it appears that complete ligand removal places Pd^{2+} in the sodalite cages (*10*). The reducibility of metal ions after calcination is determined by the degree of lattice stabilization of the ion, which is related to metal ion location. TPR data show that the ease of reduction of metal ions decreases in the following order: supercages > sodalite cages > hexagonal prisms (*1, 5, 10*). In addition, the resultant particle size is dependent on the reduction temperature and, therefore, on ion location prior to reduction.

In Part I of this series we studied the effect of calcination temperature on ion ex-

[1] To whom correspondence should be addressed.

0021-9517/89 $3.00

changed $Pd(NH_3)_4^{2+}$/NaY (*10*). Examination of ammine removal, relative reducibility, and subsequent H/Pd ratios as a function of calcination temperature led to the conclusion that calcination can produce two different situations.

Case I. Low-temperature calcination ($T_C \leq 250°C$) leaves $Pd(NH_3)_x^{2+}$ complexes located in the *supercages*. Reduction of these complexes yields Pd particles, the metal dispersion increasing with increasing ammine removal. This finding was rationalized in terms of a reduction mechanism involving competitive rates of nucleation and growth. Increasing ligand removal results in a stronger ion/lattice interaction yielding a lower ion mobility. This provides a higher concentration of nucleation sites and a correspondingly lower rate of growth, resulting in the formation of smaller particles.

Case II. High-temperature calcination ($T_C \geq 300°C$) places Pd ions in the *sodalite cages* where reduction is more difficult. After gentle reduction, the resultant H/Pd ratios are substantially lower than those found in case I, and they do not change with increasing calcination temperature.

The objective of the present paper is to elucidate the processes which occur during reduction of Pd ions in the supercages (case I) and in the sodalite cages (case II). Pd/NaY samples with three different metal loadings will be characterized using TPD after reduction to various temperatures. A model describing the elementary steps of particle formation and growth will be based on the experimental H/Pd ratios and TPD spectra as a function both of the reduction temperature and of the metal loading.

METHODS

B1. Sample Preparation

Three different batches (2, 4, and 7 wt%) of Pd supported on NaY were prepared by ion exchange. The exchanges were performed by adding a dilute solution (0.01 *M*) of $[Pd(NH_3)_4](NO_3)_2$ (Strem Chemicals, Lot No. 19167) dropwise to a NaY (Linde LZY-52) slurry (1 g/200 ml) at room temperature.

B2. Calcination Procedure

The calcination procedure established for Pt by Gallezot *et al.* (*11*) was shown to remove ammine ligands without autoreduction of Pd (*10*) and was used in this study. All samples were calcined under a high flow (180 ml/min) of pure O_2 in a packed bed reactor at atmospheric pressure. The temperature was ramped at 0.5°C/min from room temperature to either 250 or 500°C and then held at this temperature for 2 hr. The flow was then switched to Ar (22 ml/min) and the catalyst was cooled to RT in preparation for temperature-programmed studies.

B3. Temperature-Programmed Reduction/Desorption

TPR procedure. The apparatus used for TPR and TPD has been described in detail elsewhere (*10*). Samples consisting of 150 mg of 2 wt% Pd/NaY were used for all TPR spectra. TPR was performed after calcination to 250 or 500°C and after reoxidation of a reduced sample at 100°C for 1 hr. The samples were cooled to −80°C in Ar; then the flow was switched to 5% H_2/Ar (flow rate 25 ml/min). The temperature was ramped from −80 to 350°C at 8°C/min.

TPD procedure. Calcined samples were reduced under a 5% H_2/Ar flow (25 ml/min) with a temperature ramp of 8°C/min to the respective reduction temperature, then held in the H_2/Ar flow at this temperature for 15 min. H_2 consumption during reduction was monitored; this number was used in calculating the H/Pd^0 ratios (assuming reduction of Pd^{2+} to Pd^0). This method eliminates errors due to weighing and keeps the experimental error of the H/Pd^0 values within 10%.

Hydrogen chemisorption prior to TPD followed a standardized procedure: the sample was allowed to cool to room temperature in the H_2/Ar flow and then held in this flow for 15 min to ensure complete coverage. The sample was then purged in an Ar flow (22 ml/min) at room temperature for 20 min to guarantee complete destruction of

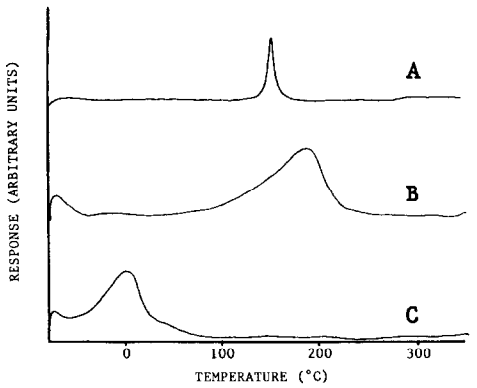

FIG. 1. TPR spectra of 2 wt% Pd/NaY samples after the following pretreatment conditions: (A) calcined to 250°C; (B) calcined to 500°C; (C) calcined to 500°C, reduced to 350°C, reoxidized to 100°C.

the Pd hydride phase (*12*). Finally, the sample was cooled to −80°C in preparation for the TPD, which was performed in an Ar flow (22 ml/min) with a temperature ramp of 8°C/min from −80 to 700°C.

RESULTS

C1. TPR

Figure 1 shows the TPR profiles for reduction of three well-defined Pd species. Spectrum A of a sample calcined to 250°C is typical for $Pd(NH_3)_x$ ions in supercages. Spectrum B of a sample calcined to 500°C is characteristic of naked Pd^{2+} ions in the sodalite cages, primarily in the SI′ sites. In both cases we refer to our previous paper and Gallezot's data for the identification of the Pd species (*10, 13*). Spectrum C of the sample used in spectrum B, after reoxidation at 100°C for 1 hr, characterizes reduction of PdO particles. *In situ* mass spectrometric analysis during reduction of spectra B and C confirms that substantial amounts of water are desorbed *only* in the case of spectrum C. In Table 1 the positions of the TPR peak maxima are given for the three different loadings after calcination to 250 or 500°C. It can be seen that, in the case where T_C = 250°C, the reduction rate maxima occur at the same temperature, irrespective of the metal loading. For the case where T_C = 500°C, however, the reduction rate maxima shift to lower temperatures with increasing Pd loading.

TABLE 1

Pd Loading	TPR peak maxima (°C)	
	T_C = 250	T_C = 500
2.0	153	190
4.3	149	167
6.7	150	150

C2. TPD

Figure 2 shows the TPD spectra of samples, all of which contain 2 wt% Pd and have been calcined to 250°C and then reduced to temperatures which are different for each sample. H_2 consumption during reduction was monitored and in all cases corresponds to complete reduction of Pd^{2+}. Previously, it has been shown that the peak

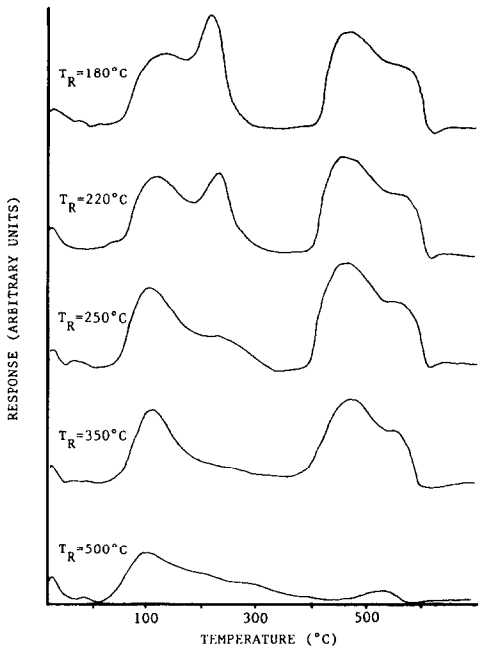

FIG. 2. TPD spectra of 2 wt% Pd/NaY samples after calcination to 250°C and reduction to various temperatures.

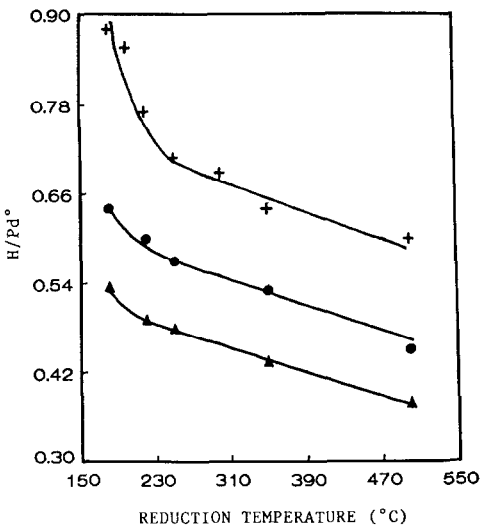

FIG. 3. H/Pd^0 ratios obtained after calcination to 250°C plotted against the respective reduction temperatures for three weight-loading Pd/NaY samples: +, 2 wt%; ●, 4 wt%; ▲, 7 wt%.

at $T \geq 350$°C in these TPD spectra is due to the decomposition of NH_4^+ ions which are formed during reduction of the $Pd(NH_3)_x^{2+}$ ions left after calcination at 250°C (*10*). This peak must, therefore, be disregarded when the amount of desorbed H_2 is calculated. The most distinctive features of this series of TPD spectra is the presence of two maxima for desorption of H_2. The low-temperature peak has a maximum at 100°C and the high-temperature peak at 210°C. The TPD spectra of the 4 and 7 wt% samples are similar in appearance and peak positions and are not shown here. The H/Pd^0 ratios calculated from the TPD spectra for the 2, 4, and 7 wt% samples are plotted as a function of the reduction temperature in Fig. 3.

The TPD spectra of the 2 wt% Pd sample after calcination to 500°C and reduction to various temperatures are given in Fig. 4. Peaks at $T \geq 350$°C, due to decomposition of NH_4^+ ions, are, of course, absent from these spectra. Therefore, total integration of the spectra in Fig. 4 provides all H_2 desorbed from which the H/Pd^0 ratios are then calculated. As in the previous case, the TPD spectra for the higher loading samples are similar and are not shown. The H/Pd^0 ratios for the 2 and the 7 wt% samples are displayed in Fig. 5 as a function of the reduction temperature.

DISCUSSION

D1. Reduction Processes of Pd in NaY

Spectra A and B in Fig. 1 are the TPR profiles characteristic for reduction of Pd ions in supercages and in sodalite cages, respectively. The distinct differences in these two spectra suggest different reduction processes for Pd ions in these two locations. The sharp, symmetric TPR peak profile in spectrum A and its position at a lower temperature suggest a rather low activation energy and a uniform barrier for reduction of Pd ions in the supercages. A higher activation energy for reduction of Pd ions in sodalite cages is suggested by the peak position of spectrum B. The broad, asymmetric shape of this TPR peak is indicative of a nonuniform reduction process. In addition, the dependence of the peak positions on the

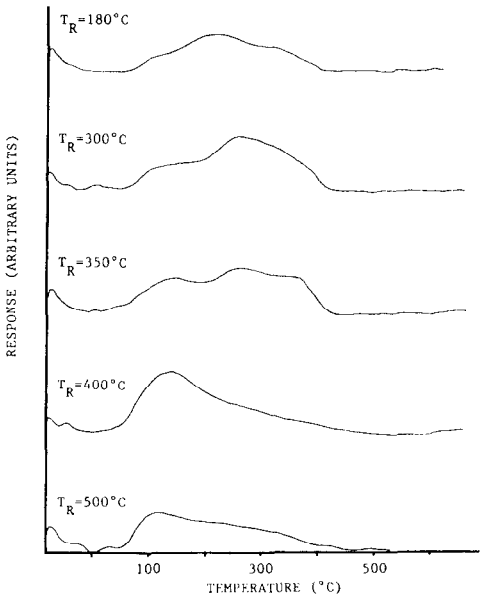

FIG. 4. TPD spectra of 2 wt% Pd/NaY samples after calcination to 500°C and reduction to various temperatures.

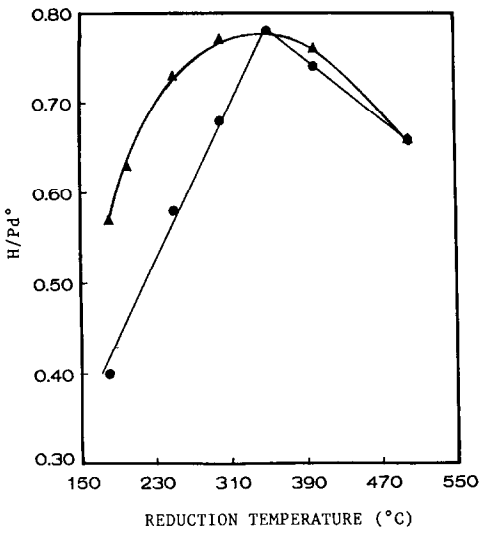

FIG. 5. H/Pd^0 ratios obtained after calcination to 500°C plotted against the respective reduction temperature for three weight-loading Pd/NaY samples: ▲, 2 wt%; ●, 7 wt%.

metal loading is relevant: Table 1 shows that for Pd ions in the supercages, the reduction rate maximum does *not* change with metal loading; but for Pd ions in the sodalite cages the peak does shift to lower temperatures with increasing Pd concentration. A drastically lower peak temperature is characteristic of spectrum C in Fig. 1, which has been attributed to reduction of PdO particles. These results can be rationalized by considering elementary principles of thermodynamics and their implication for the reduction processes for the three cases.

Case I: Pd ions in supercages. Previous data suggest that metal ion reduction and particle formation are concerted processes for reduction of Pd ions in the supercages (*10*). The metal–metal bond formation obviously provides a strong thermodynamic driving force for reduction. The fact that varying the metal load has no apparent effect on the activation barrier (TPR peak maxima given Table 1) is in conformity with facile particle formation.

Case II: Pd ions in sodalite cages. In this case, the data suggest that reduction uses a different pathway. X-ray analysis of Pt/NaY and Pd/NaY has shown that reduction of the metal ions in sodalite cages leaves initially reduced Pt or Pd atoms trapped inside these cages (*11*, *14*). For isolated atoms or pairs of two atoms, the enthalpy contribution due to metal–metal bond formation will obviously be either absent or drastically lower than when larger clusters are formed, e.g., in the supercages. The lower enthalpy of ions, which are stabilized in small zeolite cages in conjunction with the higher enthalpy of forming isolated atoms or pairs, thus implies a less exothermic or even endothermic reduction process. Its main driving force is, presumably, the strong interaction of the protons with the oxygen ions of the cage wall. As is often the case in chemistry, a lower driving force implies a lower reaction rate and a higher activation energy.

The present finding, that the position of the TPR peak maxima decreases with increased loading, also agrees with the concept that ions are reduced inside the small cages. When assuming a homogeneous dispersion of metal ions throughout the zeolite after calcination, it follows that the 2, 4, and 7 wt% metal loadings correspond to 0.4, 0.9, 1.4 Pd ions per sodalite cage. Therefore, in the low-loading regime, the chance for two Pd ions to occupy the same sodalite cage is small, but in the high-loading case it is obvious that a significant fraction of the sodalite cages will contain *two* Pd ions, one presumably occupying the SI′ site (*14*) and the other in the SII′ position. There is evidence in the literature for pairs of, e.g., La ions, coupled via a hydroxyl bridge, in sodalite cages (*15*). Reduction of a pair of Pd ions, leading to formation of a Pd–Pd bond, is thermodynamically, much more favorable than formation of an isolated atom, which can interact with its cage wall only by van der Waals forces. Again, the process which is more favorable energetically should occur at a lower temperature. The asymmetric TPR peak profile is

then tentatively ascribed to the simultaneous presence of two reduction processes, viz. isolated Pd ions and ion pairs, both in sodalite cages. The observations are in conformity with this model: the TPR peak is located at lower temperature for higher metal loadings (see Table 1).

Case III: Reduction of PdO. IR spectroscopy has demonstrated that reduction of Pt ions in Y zeolites is accompanied by formation of zeolite protons, as expected (*1, 16*). It is generally agreed that the same will be true for reduction of Pd ions, and this has been confirmed by the absence of H_2O production during reduction of a Pd/NaY sample calcined to 500°C. Reoxidation at low temperature after reduction of Pd particles in supercages should yield PdO. However, Gallezot *et al.* reported that reoxidation of small Pd particles in Y-type zeolite can result in the formation of Pd ions (*14*). Our recent data show that this redispersion into ions is temperature dependent and occurs in two steps: formation of PdO is followed by its reaction with zeolite protons yielding H_2O and Pd^{2+} ions (*17*). After gentle reoxidation at 100°C TPR displays a characteristic peak at very low temperatures (spectrum C). That this peak is, indeed, due to reduction of PdO follows from mass spectrometric analysis, which shows that a substantial amount of H_2O is produced during this reduction. Virtually no H_2O is detected during spectrum B. The peak position of C is also in agreement with thermodynamic expectation, since formation of H_2O largely contributes to the "driving force" of the reduction process.

D2. Particle Growth Processes

The large differences between reduction of Pd ions in supercages (case I) and in sodalite cages (case II) are not only evident from the TPR data; even more striking differences emerge from the dependence of the metal dispersion on the reduction temperature. The H/Pd^0 ratios are plotted in Fig. 3 and Fig. 5 against the reduction temperature. From these figures it is obvious that the particle migration and growth processes are vastly different.

Case I: Pd ions in supercages. As very few supercages will contain more than two Pd ions, it is visualized that reduction will initially result in small "primary" particles. As these will be smaller than the apertures between supercages, their migration is not impeded by the zeolite structure. Migrating primary particles with diameters $d < 7$ Å can thus easily coalesce to larger particles. Secondary particles ($d \geq 7$ Å) are unable to pass through the windows which separate supercages from each other; therefore, these trapped particles should be more stable at higher reduction temperatures than the primary particles. Support for this model is found in the characteristic shape of the curve in Fig. 3, showing H/Pd^0 vs reduction temperature for the 2 wt% sample. It is obvious that a steep drop is followed by a much slower decrease in dispersion. Evidently, two growth mechanisms are operative: first the fast disappearance of the primary particles, then a much slower growth due to some high activation energy process. For samples with higher metal loading the first process of particle coalescence is even faster, so that the first steep drop in H/Pd^0 is no longer observed.

This model is further supported by the TPD spectra in Fig. 2. The reader is reminded, that the high-temperature part of the spectra in Fig. 2 is due to decomposition of residual ammonia for the samples which had been calcined at low temperature. Only the low-temperature part of these TPD spectra is indicative of hydrogen desorption and particle size. This part of the TPD spectra reveals two hydrogen desorption peaks for samples reduced at low temperature. The area under the first (low temperature) TPD peak (T_{max} = 100°C) remains constant for low reduction temperatures, but decreases at high T_R. Conversely, the second TPD peak (T_{max} = 210°C) decreases rapidly at low reduction temperatures and is absent for $T_R \geq 300$°C. It is tempting to assume that this peak cor-

responds to hydrogen desorption from the primary particles; their number decreases as the reduction temperature is increased. Hydrogen adsorption is stronger on the primary than on the secondary particles because the metal atoms of the former entities have a high degree of coordinative unsaturation, and their electronic properties differ from those of bulk metals. Chou and Vannice found that the heat of adsorption of H_2 remains constant for Pd particle sizes ranging from 10,000 to 30 Å but increases sharply as the particle size decreases further (*18*). It is also interesting to note that a similar bimodal particle-size distribution was found by SAXS for a Pd/NaY catalyst, which had been calcined and reduced to 277°C (*19*).

The mechanism of particle formation and growth starting from Pd ions in supercages can now be summarized as follows: Pd ions migrate to an activated nucleus where they are reduced, forming primary particles. These migrate through the supercage network until they either contact another primary particle or a secondary particle. Once all the primary particles are used up, further growth of the secondary particles occurs via a different mechanism, possibly involving Ostwald ripening or local collapse of the zeolite matrix.

Case II: Pd ions in sodalite cages. The plot of H/Pd^0 vs reduction temperature after T_c = 500°C is shown in Fig. 5. At this point, it should be stressed that the dispersion data are expressed in terms of *reduced* Pd, calculated from the hydrogen consumption during reduction. The striking difference between the shape of this curve and the H/Pd^0 curve in Fig. 3 evidently shows that the mechanisms of reduction and particle migration are totally different in both cases. We previously quoted data showing that reduction of ions inside sodalite cages initially yields either isolated atoms or very small clusters (presumably dimers). Their escape from the small cages through the O_6 ring ($d \approx 2.2$ Å) is likely to be difficult, as the atomic diameter of a Pd atom ($d \approx 3.4$ Å) is much larger than the rigid model diameter of the cage window ($d \approx 2.2$ Å). Only lattice vibration at elevated temperature permits the escape of these atoms or pairs.

This model is supported by TPD data and H/Pd^0 ratios as a function of reduction temperature, if it is assumed that isolated Pd atoms in sodalite cages are unable to dissociatively chemisorb H_2. Several authors observed that reduced metal atoms trapped in sodalite cages are incapable of chemisorbing H_2. Gallezot *et al.* used SAXS and H_2 chemisorption to examine a Pt/NaY sample with the majority of reduced Pt atoms trapped in sodalite cages. The X-ray data indicated nearly atomic dispersion, but H/Pt was only 0.25 (*11*). Kubo *et al.* also reported a case where the largest Pt particles in Pt/NaY which could be detected by electron microscopy had a size of 15 Å, but the particle size calculated from H_2 chemisorption was 1300 Å (*20*). In another paper, Gallezot *et al.* say that isolated Pd atoms in the sodalite cages were unable to chemisorb H_2 (*13*). Although the steric difficulty of hydrogen molecules to pass through the O_6 ring might contribute to this, we do not believe that this is decisive in this case, because Pd ions in sodalite cages can be reduced with H_2 at elevated temperatures. It is possible that dissociative chemisorption of H_2 requires an ensemble of two or more atoms. This seems reasonable in view of theoretical calculations showing that dissociation of H_2 on isolated Ni atoms has a prohibitively high activation barrier (42 kcal/mol) (*21*).

We, therefore, will further assume that particles in supercages are capable of chemisorbing H_2, but particles in sodalite cages are not. The increase in H/Pd^0 with reduction temperature at low temperatures ($T_R \leq 350$°C) in Fig. 5 is then indicative of the activated release of reduced Pd from the sodalite cages. An activated escape of reduced Pd atoms from the sodalite cages has been observed before by Gallezot *et al.* They used benzene hydrogenation as a probe reaction on Pd/NaY catalysts that

were calcined and reduced so as to leave the majority of metal atoms trapped in sodalite cages (*22*). The rate per unit mass of Pd increased with increasing reduction temperature passing through a maximum at 350°C, similar to the present curve. Analogous behavior was also found for Pt/NaY catalysts using both benzene hydrogenation and H_2 chemisorption (*23*). The increase in Pd available for chemisorption outweighs any loss in dispersion due to particle agglomeration until T_R = 350°C. At this point the majority of Pd has been released from the sodalite cages. Upon further raising the reduction temperature, traditional particle migration and agglomeration behavior control the change of H/Pd^0 ratio.

The TPD profiles in Fig. 4 add further support to this conclusion. For low reduction temperatures ($T_R \leq 350$°C) the TPD spectra are broad and not well-defined, but for $T_R \geq 350$°C the TPD profiles display the same low-temperature desorption peak, which has been observed (Fig. 2) and attributed to the existence of secondary particles. In fact, the TPD spectra for T_R = 500°C are identical for both the T_C = 250°C and T_C = 500°C cases.

It should be mentioned that the samples with the same metal loading, which were calcined at different temperatures but reduced at the same temperature, show different metal dispersions [compare, e.g., for 2 wt% Pd (T_C = 250°C, T_R = 350°C) H/Pd^0 = 64%, but for 2 wt% Pd (T_C = 500°C, T_R = 350°C) H/Pd^0 = 78%]. This reflects the significant difference in mechanism by which metal particles are formed, either exclusively from ions in supercages or with participation of isolated Pd atoms escaping from sodalite cages. In either case nucleation and growth at low temperature lead to very small "primary" Pd particles in supercages. Before they reach the critical size defined by the apertures between supercages, they can move rather freely at reduction temperatures near 230°C; coalescence of such primary particles with each other is assumed to be responsible for the initial steep decrease in dispersion shown in Fig. 3, and for the formation of "grape-shaped" particles, observed by Gallezot *et al.* (*14*). However, when primary particles are exposed to a shower of Pd atoms which escape from sodalite cages into supercages, a new route is open for the particles to reach the critical size, where they become trapped in their supercages. In the absence of these atoms, primary particles with sizes just below the critical dimensions of the cage window can only grow by coalescence with similar particles; i.e., they will double in size and often form "grapes" connected through necks between two adjacent supercages. When exposed to a shower of atoms escaping from the sodalite cages, the primary particles can reach the critical size by simply trapping one or two atoms. As a consequence, the trapped particles in supercages will be smaller, and formation of grape-shaped particles will be improbable. This model is consistent with our earlier findings with bimetal/zeolite systems, where Pt nuclei are growing by trapping Cu ions (*24*) or Re atoms (*25*). It is also conceivable that some Pd atoms which leave sodalite cages will collide with each other and form additional nuclei, thus further increasing the metal dispersion.

CONCLUSIONS

The processes leading to Pd particle formation during reduction with H_2 strongly depend on the location of the Pd ions, which is controlled by the calcination conditions. When Pd ions are left in the supercages, primary Pd particles are easily formed. They migrate and coalesce to form secondary particles at higher temperatures. Reduction of Pd ions in the sodalite cages produces isolated Pd atoms or very small clusters inside these cages. Pd atoms are released into the supercage network at higher temperatures, where they form secondary particles either through migration and coalescence or by trapping Pd atoms as they leave the sodalite cages.

ACKNOWLEDGMENTS

We gratefully acknowledge support from the U.S. Department of Energy under Contract DE-FG02-87ERA3654. A grant-in-aid by the Engelhard Corp. is also gratefully acknowledged.

REFERENCES

1. Tzou, M. S., Teo, B. K., and Sachtler, W. M. H., *J. Catal.* **113,** 220 (1988).
2. Moretti, G., and Sachtler, W. M. H., *J. Catal.*, in press.
3. Moretti, G., and Sachtler, W. M. H., *J. Catal.*, in press.
4. Balse, V. R., Sachtler, W. M. H., and Dumesic, J. A., *Catal. Lett.* **1,** 275 (1988).
5. Tzou, M. S., Jiang, H. J., and W. M. H. Sachtler, *React. Kinet. Catal. Lett.* **35,** 207 (1987).
6. Park, S. H., Tzou, M. S., and Sachtler, W. M. H., *Appl. Catal.* **24,** 85 (1986).
7. Tzou, M. S., Jiang, H. J., and Sachtler, W. M. H., *Appl. Catal.* **20,** 231 (1986).
8. Tzou, M. S., Teo, B. K., and Sachtler, W. M. H., *Langmuir* **2,** 773 (1986).
9. Jiang, H. J., Tzou, M. S., and Sachtler, W. M. H., *Appl. Catal.* **39,** 255 (1988).
10. Homeyer, S. T., and Sachtler, W. M. H., *J. Catal.* **117,** 91 (1989).
11. Gallezot, P., Alarcon-Diaz, A., Dalmon, J. A., Renouprez, A. J., and Imelik, B., *J. Catal.* **39,** 334 (1975).
12. Hwang, H. S., and Boudart, M., *J. Catal.* **39,** 44 (1975).
13. Gallezot, P., and Imelik, B., *Adv. Chem. Ser.* **121,** 66 (1973).
14. Bergeret, G., Gallezot, P., and Imelik, B., *J. Phys. Chem.* **85,** 411 (1981).
15. Mauge, F., Gallezot, P., Courcelle, J.-C., Engelhard, P., and Grosmangin, J., *Zeolites* **6,** 261 (1986).
16. Dalla Betta, R. A., and Boudart, M., *in* "Proceedings, 5th International Congress on Catalysis, Palm Beach, 1972" (J. W. Hightower, Ed.), p. 1329. North-Holland, Amsterdam, 1973.
17. Homeyer, S. T., and Sachtler, W. M. H., *Appl. Catal.* (in press).
18. Chou, P., and Vannice, M. A., *J. Catal.* **104,** 1 (1987).
19. Moraweck, B., Clugent, G., and Renouprez, A., *J. Chem. Phys.* **83** (1986).
20. Kubo, T., Arai, H., Tominaga, H., and Kunugi, T., *Bull. Chem. Soc. Japan* **45,** 607 (1972).
21. Ruette, F., Blyholder, G., and Head, J., *J. Chem. Phys.* **80,** 2042 (1984).
22. Bergeret, G., Tri, T. M., and Gallezot, P., *J. Phys. Chem.* **87,** 1160 (1983).
23. Gallezot, P., Datka, J., Massardier, J., Primet, M., Imelik, B., *in* "Proceedings, 6th International Congress on Catalysis, London, 1976" (G. C. Bond, P. B. Wells, and F. C. Tompkins, Eds.), Vol. 2, p. A11. The Chemical Society, London, 1976.
24. G. Moretti and W. M. H. Sachtler, *J. Catal.* **115,** 205 (1989).
25. C. M. Tsang, S. M. Augustine, J. B. Butt, and W. M. H. Sachtler, *Appl. Catal.* **46,** 45 (1989).